Assessing the Use of AM - Advanced Space Additive Manufacturing Applied to High Tech Control Valves

ESA Contract No. 4000137618/22/NL/GLC/idb

Giacomo Cappelli [1], Patrick Walsh [2], David O'Dwyer [2], Rocco Lupoi [1]

[1]Trinity College Dublin, The University of Dublin, Department of Mechanical, Manufacturing & Biomedical Engineering, Dublin, Ireland

[2]SchuF Ireland, Cork, Ireland

Abstract

This study proposes the assessment of impingement erosion and electrochemical corrosion resistance of two coatings materials deposited by Cold Spray technology and compare them to 440C annealed steel. The tested coating materials were CrMnFeCoNi and WC-Ni, deposited on 2205 duplex stainless steel substrates using nitrogen as process gas. In between the substrate and the high entropy alloy coating, an interlayer coating of 316 stainless steel was used to enable HEA adhesion. The presence of WC particles in the WC-Ni composite coatings was confirmed by SEM cross sectional inspection. Following deposition, the coatings were heat treated in an air furnace. The influence of heat treatment holding time on the WC-Ni coatings was studied using chemical analysis by x-ray diffraction. Heat treatments peak temperatures for the WC/Ni-Ni and high entropy alloy coatings were 600°C and 550°C, respectively. Coatings microhardness and porosity volume fraction were measured for all the samples. The HEA coating outperformed the WC/Ni-Ni hardness but exhibited a higher level of porosity. Both the coatings and 440C plates were then subjected to erosion experiments using alumina particles with variable impact angles (30°, 60°, and 90°). To compare the different materials, an average erosion value was calculated for each target specimen. The WC/Ni-Ni as-sprayed coating was the most effective coating against a 60° impingement angle. The HEA coating, on the other hand, demonstrated greater resistance to impact angles of 30° and 90°. However, the 440C substrate seems to be more resistant to particles impingement. Cyclic Potentiodynamic tests were also conducted on the three different materials and the 440C showed the highest corrosion rate. In this study the Selective Laser Melting processing of 316 stainless steel and Maraging steel was conducted. Optimal parameters were defined by DoE approach and the mechanical behaviour of the manufactured parts was tested.

Introduction

Cold Spray coatings in valve components

Erosion problems are common in pneumatic and hydraulic systems due to the action of the processed mean. Sometimes this issue can be faced with design refinements changing the system at a base level. On the other hand, when design changes are not possible or not enough for preventing the problem, the selection of the proper material is of main focus. To further improve components toughness and wear resistance, hard material coatings are substantially applied using thermal spray methods such as laser cladding[1], plasma spray[2], high-velocity oxyfuel[3], and cold spray[4]. The most common coating material named as "cermets" consist of hard particles such as tungsten carbides or alumina oxides dispersed in a metal matrix usually made of cobalt or nickel.

Cold spray is an additive manufacturing process characterized by high deposition mass rate and low thermal stresses, while it can efficiently fabricate dense and thick metallic coatings[5]–[7]. However, the principle at the base of the particles adhesion to the substrate is related to particles plastic deformation. Therefore, this principle does not apply to hard and brittle particles, that are instead entrapped in the coating as a result of the ductile matrix action. Nowadays, a few researchers tried to deposit composite cermet coatings by cold spray with the goal of increasing the deposition efficiency and the quantity of ceramic particles embedded in the resulting coatings[8]. Some of them also tested the coating resistance under wear or impingement erosion of a slurry or dry particles[4].

Solid particle erosion (SPE), in particular, is a type of erosion that occurs when solid particles dragged by fluid media impact on a surface resulting in mass loss of the target. The use of cermet coatings in the protection of metallic materials from SPE has shown promising results[9], [10] as their resistance is generally superior to that of their metal matrix. Furthermore, the cermet hard particles-ductile matrix composition ratio is an important characteristic since the SPE mechanism is strongly dependent on the impingement angle. Indeed, it has been proven that ductile materials are considered to exhibit better erosion resistance at normal impingement angle, while brittle materials at lower angles (60°, 30°) [7,15]. In addition to the impingement angle the SPE behaviour is also influenced by the erodent properties such as feed rate, velocity, size, and hardness. In the present study, we were interested in comparing the erosion resistance of CrMnFeCoNi and WC-Ni coatings to 440C martensitic steel, currently used by SchuF in many applications. During this study, an attempt was made to raise the concentration of WC in the coating, but no positive results were obtained.

As previously discussed, in the past years, wear and erosion problems have been mainly faced with the application of hard ceramic materials embedded in a metal matrix. In this study, the erosion behaviour of a cold sprayed high entropy alloy (HEA), in particular the Cantor CrMnFeCoNi was tested. Even though HEA are becoming popular in the scientific community, the behaviour against impingement erosion of this particular alloy has not been assessed yet, being part of the novelty provided by this study.

HEAs are not easily deposited through cold spray since they require helium as process gas or really high working parameters for cold spray systems employing nitrogen[11]–[14]. However,

deposition of this material through cold spray may lead to hardness improvements due to the combination of HEAs high work hardening behaviour and the particles plastic deformation induced by the process. To boost coating adhesion, a stainless-steel interlayer was previously placed and adopted between the substrate and the HEA coating.

Selective Laser Melting in valve components

By developing additive manufacturing techniques for valve components manufacturing, the improved product shape freedom offered by this manufacturing approach would enable several improvements for flow regulation in many applications. In this study SchuF is interested in assessing the deposit quality that can be achieved by SLM printing, since this would give the company the possibility of more complex design production that would decrease the risk of cavitation thanks to an improved flow coefficient. The materials that were chosen for this work are 316 stainless steel and Maraging steel 18Ni300. Design of experiment approach was used in order to define the best set of process parameters that minimizes the defect sizes and pores concentration. Furthermore, once the optimal parameters were determined, the tensile behaviour of printed dog bone samples was tested to see how the mechanical performances changes before and after heat treatment.

Experimental procedure

Powders and substrate

The feedstock powders used for Cold Spray were produced by blending the composite powder WC/Ni (Amperit 547.074, – 45 + 15 µm) from Hoganas and pure Ni powder (– 45 + 16 µm) from Praxair. The powders were mixed at three different concentrations: 70%, 80% and 90% of WC/Ni volume fraction with the pure Ni powder as balance. The used HEA powder was CrMnFeCoNi (– 45 + 10 µm) provided by H.C.Starck. The coated substrates were as-machined 4 mm thick 2205 duplex stainless steel (1.4462) plates and cleaned with ethanol. Stainless steel 316 powder from Carpenter Additive was also adopted for the realization of an interlayer between the substrate and the HEA coatings.

For the SLM application instead stainless steel 316 powder from Carpenter Additive and maraging steel 18Ni300 from Hoganas were printed on 304 stainless steel sintering plates.

Cold spray deposition and heat treatments

For the coatings manufacturing, a custom-made cold spray system (Trinity College Dublin, Ireland) was used. The system is equipped with a powder feeder PF100WL from Uniquecoat Technologies LLC used at a powder feed rate of 80 g/min. For any feedstock material nitrogen was used as process gas, and the gas temperature and pressure were set at the highest achievable values of 900°C and 30 bar, respectively. The particles were accelerated through a WC–Co De Laval nozzle with a divergent length of 190 mm, throat diameter of 3 mm, and outlet diameter of 8 mm. The nozzle–substrate spray distance was set at 40 mm while the nozzle travel speed at 50 mm/s. For each one of the tested feedstocks, three layers were deposited following a zig-zag pattern with 1 mm of step distance between parallel lines. In the case of HEA coatings, an interlayer of about 700 µm thickness was deposited in SS316 to facilitate the adhesion of the consequent sprayed Cantor alloy powder.

After fabrication, the WC-Ni coatings were heat treated at 600°C with a heating ramp rate of 10°C/min. Dwell times of 1 h, 2 h and 3 h were performed to see if there are any microstructural changes depending on the duration. Slow cooling was performed in the furnace. Some of the SS316 interlayers were annealed before HEA deposition at 1000°C for 4 h dwell time. After HEA deposition, specimens were heat treated at 550°C for 1 h. All the heat treatments were performed in a Carbolite RHF1600 air furnace.

Material characterization

Powders and specimens were analysed at the Scanning Electron Microscope (SEM, Carl Zeiss ULTRA, CRANN). The SEM parameters were set at 5 kV of accelerating voltage and 8.5 mm of working distance. Samples cross sections were extracted using wire EDM (Excetex V440G) and then prepared using 320, 600, 1200, 2500 grinding papers and 6 to 1 micron suspended solution on polishing clothes. Colloidal silica suspension was also used as last polishing step. Microhardness measurements were performed on the polished cross-sections averaging the results of fifteen indentations conducted with a Vickers tester (ZwickRoell ZHV30). For the measurements a load of 500gf was applied for 10 seconds. Coating porosity was estimated using ImageJ software with images collected at the SEM at x250 magnification. The Trainable Weka Segmentation plugin of ImageJ was used to estimate the amount of WC particles entrapped in the deposited coatings. To evaluate the influence of heat treatments on the chemical composition of WC-Ni coatings, an X-ray-diffraction system (TBSI, Trinity College) was used. Coatings density was measured by Archimedes method using a scale apparatus equipped with a density determination kit (Ohaus Explorer). By Archimedes principle [15], the volume of the sample (V_s) and the density (ρ_s) can be expressed as:

Equation 1

$$V_s = \frac{m_s - m_{sf}}{\rho_y}$$

Equation 2

$$\rho_s = \frac{m_s}{V_s} = \frac{m_s}{m_s - m_{sf}}\rho_y$$

Where ρ_y is the liquid density and m_s and m_{sf} are the sample dry and submerged mass, respectively.

Solid particle erosion tests

Solid particle erosion tests (SPE) were conducted using angular shaped alumina erodent particles with 50 µm average size (Figure 1) carried by compressed air at the pressure of 1.5 bar. A scheme of the used apparatus is shown in Figure 5. The used nozzle has a length of 105 mm with a constant internal diameter of 3 mm. The tests were performed at room temperature and lasted 10 min for each specimen. The specimens were 30 mm

diameter coated disks. Before the erosion test, the coatings were prepared by machining until 1 mm of coating thickness was reached. Then, the specimens' surface was grinded with 320 paper and cleaned with ethanol. The SPE were conducted at 90°, 60° and 30° impacting angles and the distance between the nozzle and the target was set to 10 mm. Any test combination was repeated two times to get a more reliable estimate of the erosion behaviour. Each specimen was weighed before and after the erosion test using a 4 decimal weighing scale (Ohaus Discovery) to record the mass loss. Process time and erodent particles feed rate were recorded throughout all the tests. To compare the results of the different materials, an average erosion value ($mm^3\backslash g$) was used. The average erosion value was calculated by dividing the erosion rate (mg/s) by the abrasive flow rate (g/s) and then dividing again by the specimen density (g/cm^3) measured by Archimedes. The erosion test was conducted following the ASTM G76-18 standard[16].

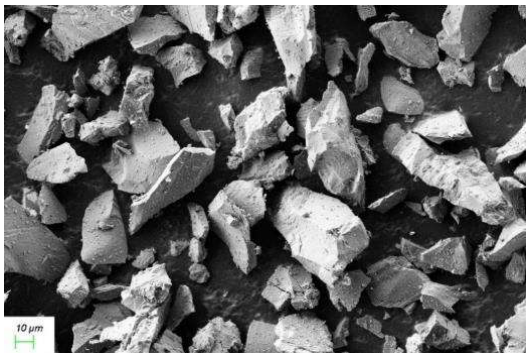

Figure 1: Alumina erodent particles.

Corrosion tests

As first instance, a qualitative corrosion test was performed following what is proposed in the standard ISO11846 – Method B typically used in automotive applications. According to the standard, specimens were immersed for 24h in a solution made of 30 g of sodium chloride, 10 ml of hydrochloric acid and 1 l of distilled water. After immersion the specimens were rinsed in running water and then distilled water. After drying, the specimens were analysed at the optical microscope.

Open circuit potential (OCP) and cyclic potentiodynamic polarization (CPP) tests were also conducted using a three-electrode system consisting of a silver/silver chloride reference electrode, a graphite counter electrode and our sample as working electrode. The electrodes were partially immersed in a NaCl solution. The tests were conducted for each material for a duration of 1 hour for the OCP to stabilize the potential and 3 hours to run the CPP test. The tests were carried out using the Gamry Framework software and the results were then analysed by Gamry Analyst. Tafel extrapolation was used to collect the corrosion potentials and currents and then to compute the corrosion rate in mils per year.

Selective Laser Melting printing

The used selective laser melting printer for the experimental tests is the ProX DMP 200 from 3D Systems. It is featured by a maximum laser power of 300W and a printing volume of 140 x 140 x 125 mm. The DOE method set of parameters for both 316 stainless steel and maraging 18Ni300 steel were randomly generated using three levels of laser power, scanning speed, and hatch distance (Figure 2). Only the combinations that fell within a 30% variation with respect to an optimal energy density that was discovered during the literature research conducted in work package 4 were considered for testing[17], [18]. All the samples were 10x10x5 mm in size. To provide higher affordability of the experimental results for each combination of parameters two samples were printed. The samples were then sectioned and removed from the build plate using wire EDM machining. The pair of samples were then hot mounted together in epoxy resin and the grinded and polished. The same procedure was carried out for SS316 and 18Ni300 steel. The samples were then examined under an optical microscope, and the optimal printing parameters were chosen based primarily on the presence and size of flaws in the examined sections. Heat treatments were applied to both the SS316 and 18Ni300 samples that showed the best properties. On the SS316 sample annealing was performed at 600°C in air with 2 hours dwell time. For the 18Ni300 steel quenching from 815°C was performed in distilled water and then the sample was left in an oven at 480°C for 6 hours for precipitation hardening procedure.

	Power [W]	Scanning speed [mm/s]	Hatch distance [mm]
316	180 - 210 - 240	800 - 1000 - 1200	0.05 - 0.07 - 0.1
Maraging	180 - 210 - 240	1000 - 1100 - 1300	0.05 - 0.07 - 0.1

Figure 2: DOE control factors and levels for SS316 and maraging steel powders.

SLM samples tensile testing

Once the ideal combination of parameters for both stainless steel 316 and 18Ni300 maraging steel was determined, two dog bones samples for tensile testing were produced for each material using those specifications. The tensile test was performed in line with the standard EN10002-1. The dog bones geometry is shown in Figure.

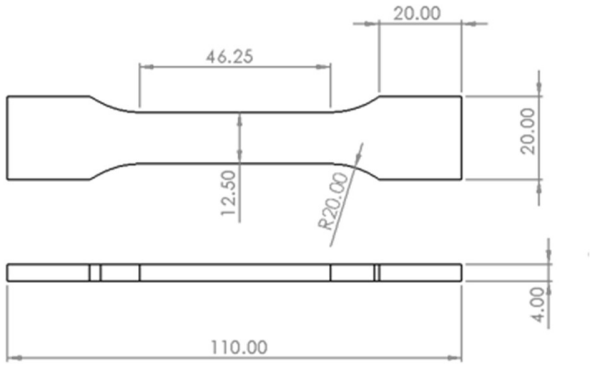

Figure 3: geometry of the dog bone samples used for tensile testing.

The tensile tests were conducted using an extensometer with 25 mm gauge length and in strain control with a rate of 0.002 s^-1 until yield condition was achieved. After yield, the test was switched in displacement control and accelerated to 3 mm\min rate.

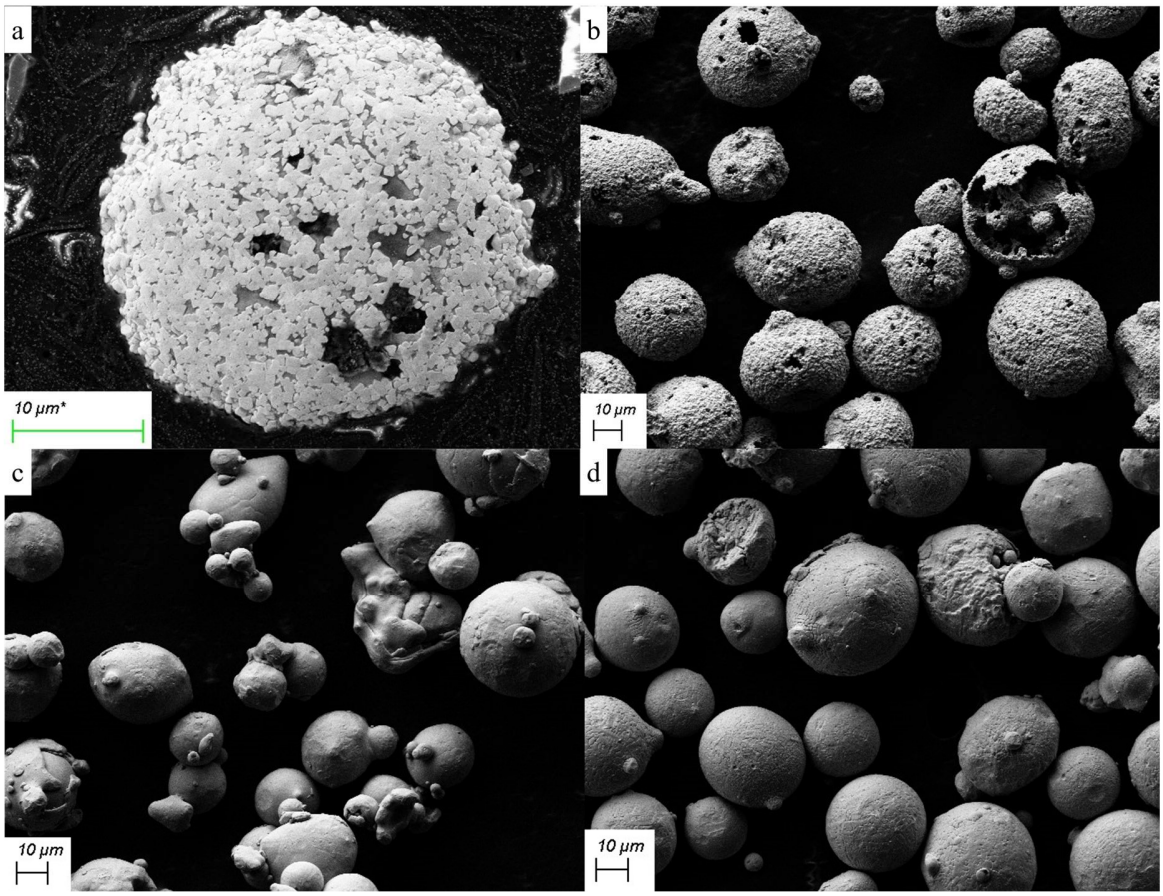

Figure 4: Electron micrographs of the feedstock powders, a) composite WC/Ni powder cross section, b) composite WC/Ni powder, c) Nickel powder, d) CrMnFeCoNi powder.

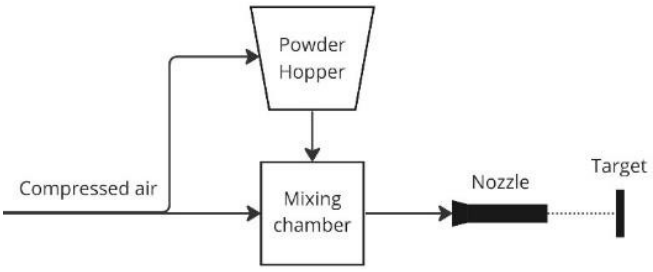

Figure 5: Solid particle erosion test apparatus.

Cold Spray application results

Powder characterization

Images collected at the scanning electron microscope of the used feedstock powders are shown in Figure 4. The WC/Ni composite powder is depicted in Figure 4a-b. This powder consists of nanosized tungsten carbide particles agglomerated in a nickel porous matrix that facilitate the powder deposition. The feedstock powder for the WC-Ni coatings was made by mixing the WC/Ni composite powder with the pure nickel powder displayed in Figure 4c. The latter is instead characterised by the typical compact and spherical morphology as in the case of the CrMnFeCoNi HEA powder shown in Figure 4d.

Coatings characterization

First of all, this study was focused on testing different WC/Ni-Ni feedstock powder compositions, increasing the concentration of WC/Ni composite powder in the feedstock from 70% of volume fraction to 90%, in line with what was done by Alidokht et al.[19] where they achieved a maximum of 54% volume concentration of WC entrapped in the coating. In the present study, deposition was obtained only when spraying the feedstock powder containing 70% volume fraction of WC/Ni powder, whereas with the 80 vol% and 90 vol% of WC/Ni concentration feedstock no deposition was obtained. A cross section of the obtained coating is shown in Figure 6a. WC particles, in light grey, are easily distinguishable with respect to the nickel matrix, darker grey areas. The average WC concentration was estimated to be 42.5±8 vol% by image analysis. In Figure 6a, small cracks are visible in the nickel matrix (red arrows), which were most likely caused by the impacting WC particles' severe compaction effect on the nickel matrix. Cracks, on the other hand, were no longer detectable in the specimens subjected to heat treatment (Figure 6b).

Results of the chemical analysis by x-ray diffraction are displayed in Figure 7. The chemical analysis was performed on three samples of WC/Ni-Ni coatings that were subjected at different heat treatments. All of them were heat treated at the temperature of 600°C in a Carbolite air furnace, but holding time was tested at 1 hour, 2 hours and 3 hours. As a result, the XRD analysis was performed to determine whether varying

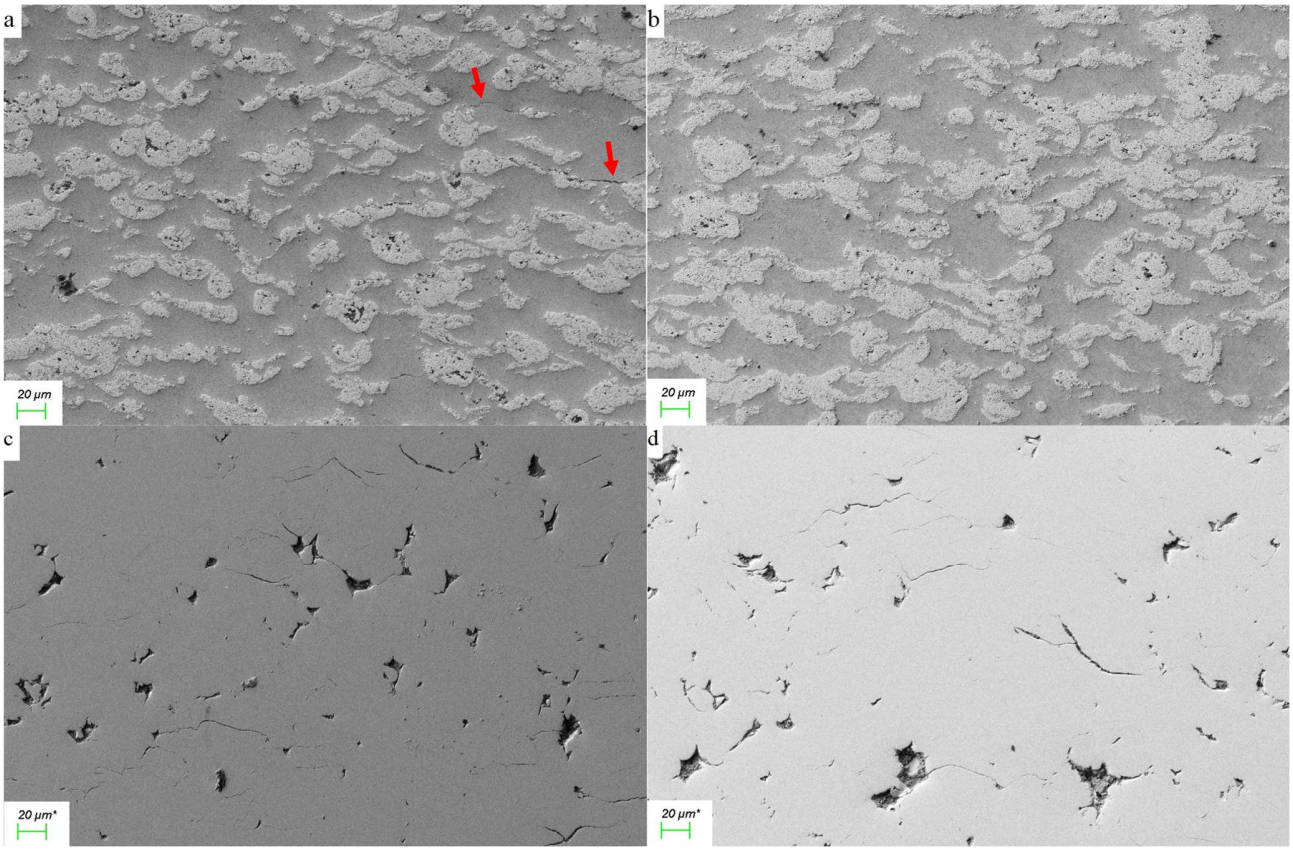

Figure 6: Electron micrographs at x250 magnification of cold sprayed coatings. a) WC/Ni-Ni coating in as sprayed condition, b) WC/Ni-Ni coating after heat treatment at 600°C for 1 hour in air, c) As sprayed CrMnFeCoNi HEA coating, d) CrMnFeCoNi HEA coating after heat treatment at 550°C for 2 hours in air.

holding times resulted in different phase changes. As can be seen in the XRD plot of Figure 7, nickel is the main component with WC, but many oxides of both nickel and tungsten were formed during the heat treatment in air. Furthermore, as can also be expected, the concentration of oxides seems to increase with the holding time. Therefore, after chemical analysis by X-ray diffraction, the selected heat treatment holding time for the WC/Ni-Ni coatings to be used for erosion testing was of 1 hour. However, no decarburization of tungsten was recorded in any of the specimens, preventing that phenomenon to be related to the holding time. Besides, the annealing heat treatment resulted to be effective in reducing the coatings porosity. Indeed, in the as-sprayed condition, the porosity was found to be 1.4±0.5 vol%, whereas in the heat-treated condition the porosity decreased to 0.7±0.2 vol%. The reduction in porosity that occurred may be related to the aforementioned crack closure and subsequent densification of the coating.

The coating microhardness in the as sprayed and heat-treated conditions were estimated as 370±58 and 252±39 HV0.5, respectively. The drop in microhardness after heat treatment is in line with what was recorded by Kazasidis et al. [20]. They attributed the cause of this drop to the nickel recrystallization that normally occurs at temperatures between 370 to 700 °C. Furthermore, the work hardening undergone by the particles during deposition might have further reduced the recrystallization temperature.

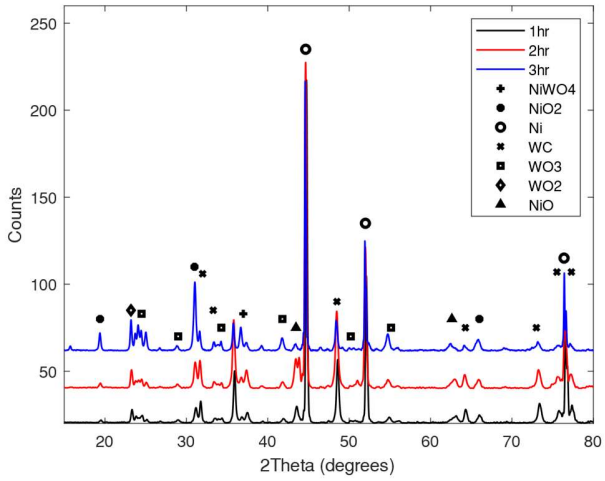

Figure 7: X-ray diffraction results of the WC/Ni-Ni coatings after heat treatment in air at 600°C varying the dwell time.

Spray tests with CrMnFeCoNi HEA powder on duplex 2205 stainless steel substrates were characterized by coating delamination that occurred periodically throughout the deposition process. Symptoms of the two materials' incompatibility. Therefore, the choice of substrate material was blamed for the unsatisfactory results. As a result, an interlayer coating made of 316 stainless steel was used to enable the HEA coating built up. The deposited stainless-steel layer was 700 µm

Table 2: Solid particle erosion tests results of WC/Ni-Ni coating in the as sprayed and heat-treated conditions.

	AS WC/Ni-Ni						HT WC/Ni-Ni					
Angle	90°		60°		30°		90°		60°		30°	
Mass loss [mg]	42	46	49	45	74	60	58	52	70	71	55	72
Erodent feed rate [g/s]	0.041	0.031	0.048	0.037	0.035	0.028	0.035	0.027	0.036	0.032	0.032	0.029

Table 1: Solid particle erosion tests results of HEA coatings on as sprayed and heat treated SS316 conditions.

	HEA on SS316						HEA on HTSS316					
Angle	90°		60°		30°		90°		60°		30°	
Mass loss [mg]	32	32	41	42	61	62	31	29	43	42	61	62
Erodent feed rate [g/s]	0.058	0.032	0.032	0.034	0.039	0.052	0.027	0.029	0.033	0.039	0.045	0.027

thick on average and was employed at the as-sprayed surface condition since the substrate roughness may promote future HEA layer adherence. However, half of the specimens were heat treated at 1000°C for 4 hours in air furnace ([21], [22]) since the softening of the 316 stainless steel interlayer might further improve the CrMnFeCoNi coating adhesion. HEA deposition was then successfully obtained on the SS316 interlayers. Subsequently, the specimens were subjected to heat treatment at 550°C for 2 hours in air furnace to release residual stresses and reduce the coating porosity. The porosity of the HEA coatings deposited on SS316, and heat-treated SS316 (HTSS316) was 1.8±0.4 vol% and 1.1±0.2 vol%, respectively. The average microhardness was 420±41 HV0.5 for the HEA deposited on SS316 and 430±50 HV0.5 for HEA coating on HTSS316 interlayer. Furthermore, the hardness of the annealed 440C resulted to be 353 HV0.5.

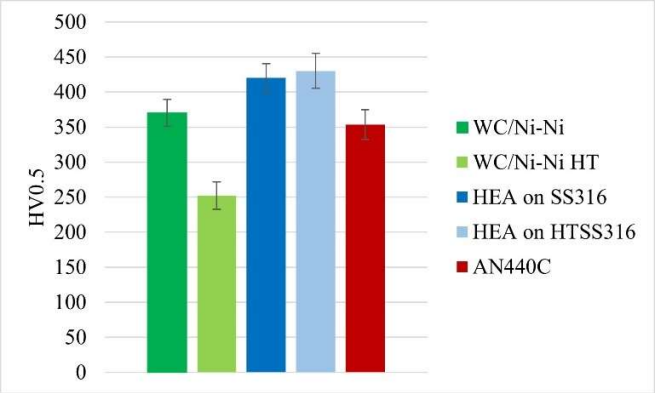

Figure 8: Microhardness HV0.5 comparison among coatings made of WC/Ni-Ni, WC/Ni-Ni after heat treatment, heat treated HEA on SS316 and heat-treated HEA on HTSS316.

Microhardness results were consistent with the ones obtained by Ahn et al. [12] who conducted an heat treatment with the same temperature and holding time in argon atmosphere. They recorded a 0.3 vol% of porosity in their coatings, that was achieved using helium as process gas. In contrast, in this study even after heat treatment, significant porosity was still present in the coatings, as can also be seen in Figure 6c-d. In the figure, microcracks, pores, and inter-particle boundaries are evident, indicating that the metallic bonding is incomplete. However, a significant reduction in porosity resulted between HEA deposition on as sprayed and heat treated SS316, illustrating the beneficial impact of the interlayer's annealed state prior to HEA deposition. The microhardness of all the deposited coatings in this study are compared in Figure 8. Despite the entrapped hard WC particles, the microhardness of the HEA coatings outperformed the composite WC-Ni coatings. That is because the overall hardness of the WC/Ni-Ni coating is the result of an average between the ductile nickel matrix and the dispersed hard particles. The diagram also shows the significant reduction in hardness of the WC/Ni-Ni coating following annealing heat treatment.

Erosion behaviour

Following the erosion test, any sample was weighed, and the mass loss due to impact erosion was determined by subtracting the post-erosion specimen mass from the pre-erosion specimen mass. In Table 1 and Table 2 the computed mass losses for any specimen under the different impacting angles are listed. Paired with the mass losses, the recorded erodent feed rates for any test are indicated. Any material-impact angle test combination was repeated two times. The majority of the coupled tests were consistent with each other since the resulting mass losses of the two repetitions were really similar. Anyway, small deviations in the mass loss were expected because of the slightly variation in the erodent feed rate throughout the experimental campaign. To make the results independent from the erodent feed rate an average erosion value that expresses the volume of the removed material per grams of sprayed erodent was computed. To do that, the coatings density was computed through Archimedes principle using Equation 2 and coating parts collected from the specimens. The estimated densities were 10.059 g/cc and 7.817 g/cc for the WC/Ni-Ni and HEA coatings, respectively. Therefore, the average erosion rate was calculated by dividing the erosion rate (mg/s) by the abrasive flow rate (g/s) and then dividing by the specimen density (g/cm^3) measured by Archimedes. The obtained results are plotted in Figure 9.

Coating erosion appears to increase when the impact angle decreases in all of the tested materials. However, the mass loss among the several test settings is less variable in the heat-treated WC/Ni-Ni coating than in the as-sprayed condition, showing a lower difference in erosion resistance among tests performed at 90°, 60° and 30° impact angles. The mass loss in the as-sprayed condition, on the other hand, is quite similar in the 90° and 60°

tests and significantly increases when the impact angle is set to 30°. In this case, what obscures the relationship between mass loss and impact angle could be the change in concentration of dispersed WC particles in the impact area.

When considering HEA coatings, the mass loss dependency on the impact angle is evident, as the mass loss grows in the same way in both material states and can be easily described by a second-degree polynomial function that rapidly increases when the angle approaches zero.

Considering the average erosion values of Figure 9, some of the aspects highlighted by the mass losses are confirmed. The heat-treated WC/Ni-Ni coating for instance shows the least variable behaviour at changes of the impact angle. Besides, erosion of the HEA coatings clearly becomes stronger as impact angle decreases. An interesting result is instead the one of the as-sprayed WC/Ni-Ni coating under 60° angle, since the average erosion is even slightly lower than the one recorded at 90° impact angle. Despite having approximately equal average hardness, HEA deposited on SS316 demonstrated to be more resistant to particle impact erosion at 30° impact angle than the same material applied on the annealed stainless-steel interlayer. Furthermore, the HEA coating deposited on SS316 showed to undergo a lower erosion under normal impact angles with respect to the HEA coating deposited on HTSS316. In this case the higher level of porosity volume fraction characterizing the HEA on SS316 coating may be the cause, since the impacting particles perform a compacting action on the coating, that deforms closing the gaps instead of losing material.

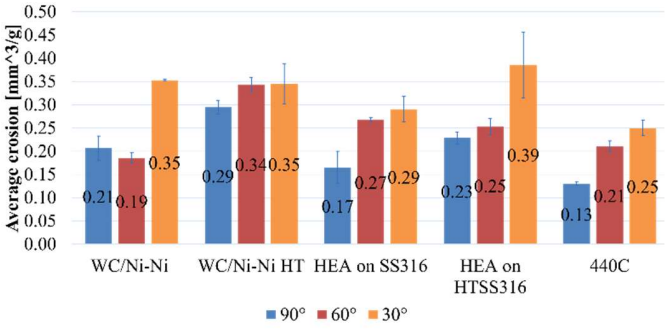

Figure 9: Average erosion results of the solid particle erosion tests conducted on WC/Ni-Ni as sprayed and heat-treated coatings, and HEA coatings on as sprayed and heat treated SS316 and 440C substrates.

From the obtained results we can conclude that the HEA coating deposited on the as-sprayed 316 stainless steel is the one showing the highest resistance against the most critical condition, that is at 30 degrees of impact angle. Furthermore, the same coating stands out when subjected to erodent particles impact at normal angle. However, at intermediate angles (60°), the WC/Ni-Ni at the as-sprayed condition was the most resistant among the tested materials.

The imprints left in any of the samples did not achieve 1 mm of depth, so the erosion process was limited to the coating and did not reach the substrate material. On average the imprints were 500 µm deep, so in line with the erosion limit imposed by the ASTME G76 – 18 standard. The imprints made on the HEA, WC/Ni-Ni coatings and 440C were all featured by a central deep zone and a round shape that is circular under 90 degrees impact angles and becomes elliptical as the angle is reduced. Similar behaviour seen in the coatings under the effect of alumina impacting particles was faced by 440C substrate. However, as shown in Figure 9 the 440C shows higher erosion resistance than the produced coatings.

Corrosion

The results of the qualitative corrosion tests are displayed in Figure 10. As can be seen from the figure, the 440C steel is almost completely covered by an oxide layer after 24 hours of immersion in the solution. On the other hand, as far as the HEA coating is concerned, the interparticle boundaries are highlighted after immersion, as is the case with the chemical etching procedure, where the grain boundaries are attacked at a faster rate than the actual grains due to the higher energy content of the grain boundaries. In contrast, the WC/Ni-Ni coating appears almost intact after 24 hours. The results obtained from this test might suggest that the corrosion resistance of 440C against the attack of a NaCl and HCl solution is lower than that of the HEA and WC/Ni coatings.

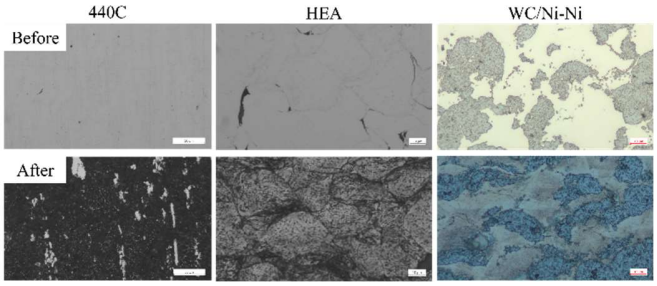

Figure 10: Qualitative corrosion test results for 440C steel, HT HEA deposited on AS SS316 and AS WC/Ni-Ni coating.

More detailed and specific corrosion tests were then performed to obtain a quantitative estimate of the corrosion resistance of the materials under investigation. The open circuit potential (OCP) recorded trends were analyzed with Gamry Analyst software and then plotted using MATLAB. OCP and CPP results are shown in Figure 11. The corrosion potential, corrosion current and corrosion rate were all obtained by Tafel extrapolation from the cyclic polarization diagrams obtained during the test. The corrosion potentials indicated in figure are the potentials at which corrosion began for each material, meaning it is a measure of how susceptible the material is to corrode. The corrosion current is generally higher for higher corrosion rates since it is related to the electrons traveling from one electrode to the other. Important is the resulting corrosion rate expressed in mm of depth per year. The 440C steel is clearly behaving worse than the other materials showing an increment of 160% in corrosion rate with respect to the lowest value recorded by the WC/Ni-Ni coating. The HEA coatings behaved quite well, showing a corrosion rate even similar to the WC/Ni coating that as expected looks to be the best against corrosive actions. Comparing the obtained results with what is recorded in literature the performed tests seem to be reliable. In literature the same test was applied to 440C characterized by martensitic structure [23], while in our case the 440C has been annealed around 800°C and therefore some austenite phase is expected. Considering the results provided in literature, corrosion potential -485 mV and corrosion current 15.0

µA/cm^2, suggest that 440C in the hard martensitic composition is more prone to corrosion than at the annealed state. The 440C grade that is currently used by SchuF is not at the annealed state and even though its erosion behaviour might be better than the annealed state it would probably be more affected to corrosion.

Material	Open circuit potential [mV]	Corrosion current [µA/cm²]	Corrosion potential [mV]	Corrosion rate [mpy]	Corrosion rate [mm/y]
440C (annealed 800°C)	-365	4.47	-307	2.04	0.052
HEA	-256	2.59	-373	1.17	0.030
HEA on HTSS	-278	1.95	-352	0.88	0.022
WC/Ni-Ni	-178	2.31	-263	0.78	0.020
HT WC/Ni-Ni	-191	3.11	-303	1.05	0.027

Figure 11: OCP and CPP corrosion tests results for 440C annealed steel, HT HEA deposited on AS SS316, HT HEA deposited on HT SS316, AS WC/Ni-Ni, HT WC/Ni-Ni.

Selective Laser Melting results

Powder characterization

The electron micrographs of the maraging steel 18Ni300 and stainless steel 316 that have been tested at the selective laser melting printer are depicted in Figure 13. As can be seen, both the powders present a mainly spherical morphology.

Printed samples characterization

The printed samples were cross sectioned and polished for micro structural analyses using the same devices previously described for the cold spray coatings. The same procedure was performed for both maraging 18Ni300 and SS316 samples. Some of the samples were characterised by presence of defects in form of elongated pores or cracks due to thermal stresses induced by the manufacturing process. An example of the recorded defects is displayed in Figure 12. The results of the micro structural analysis are listed in the table below for both SS316 and 18Ni300 DOE. The pores or defect maximum size for each sample was recorded in addition to the average porosity and micro hardness. The selection of best set of parameters was carried out by choosing the sample with the smallest defect size and then considering the level of porosity. The optimal energy density for printing the SS316 resulted to be 100 J/mm^3 as was obtained in literature. Instead for the 18Ni300 maraging steel powder the optimal value resulted to be 114 J/mm^3 even though samples printed at 90 J/mm^3 also showed good quality results. After the heat treatment, the SS316 sample microhardness slightly decreased from 265 HV0.5 to 255 HV0.5 while in literature the opposite trend was recorded. For the 18Ni300 alloy, the treatment significantly increased the sample hardness that jumped from 399 HV0.5 to 566 HV0.5.

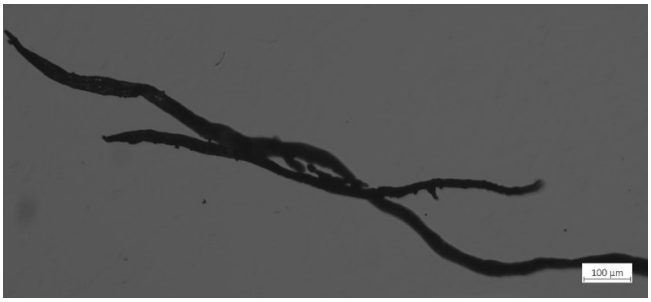

Figure 12: example of defect found in a 316 printed sample.

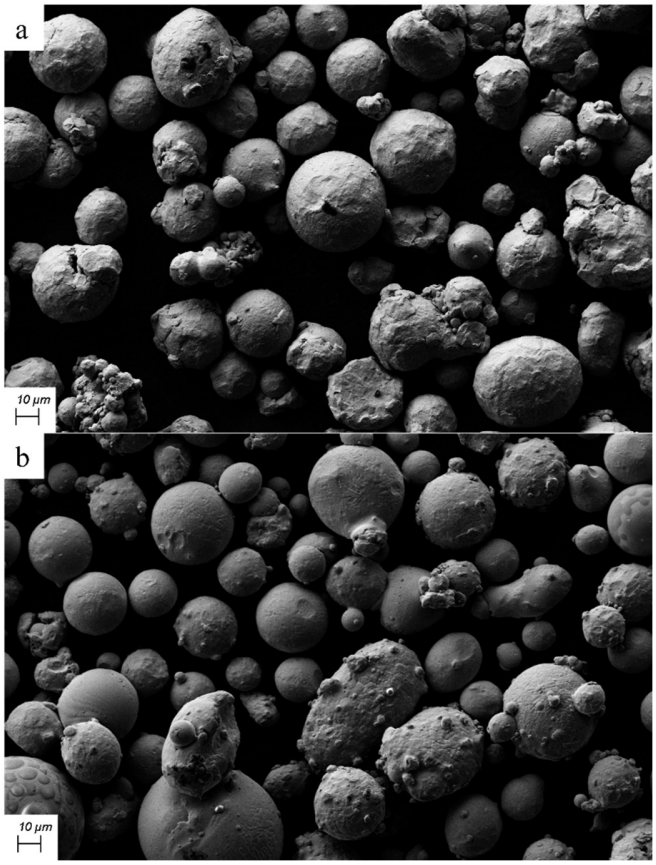

Figure 13: a) Maraging steel powder, b) Stainless steel 316 powder.

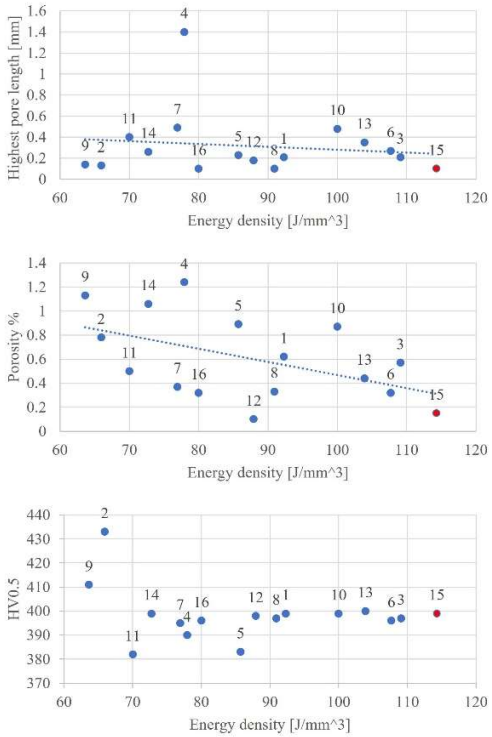

Figure 14: DOE Maraging steel results. The 15th sample was chosen as best set of parameters using a power of 240W, 1000 mm/s scanning speed and 70 µm hatch.

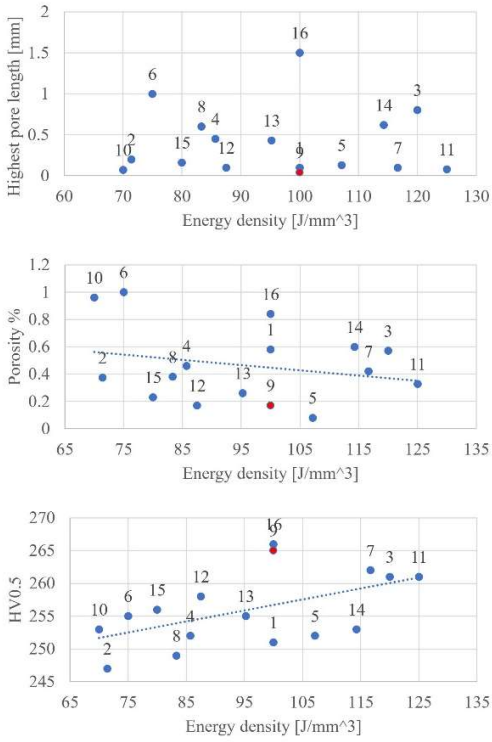

Figure 15: DOE 316 stainless steel results. The 9th sample was chosen as best set of parameters using a power of 210W, 1000 mm/s scanning speed and 70 µm hatch.

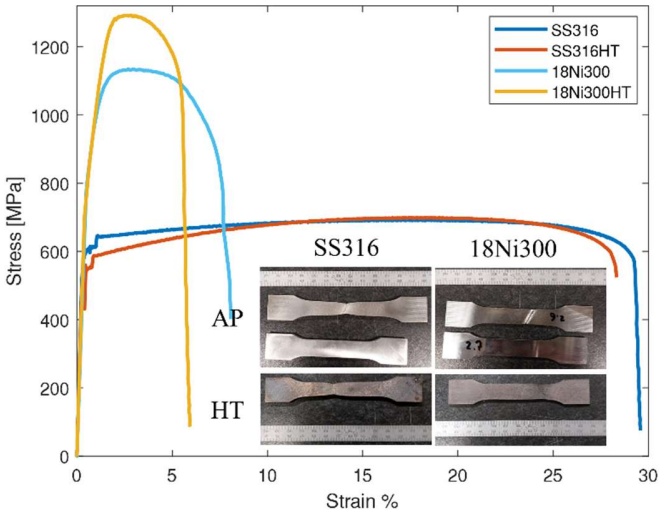

	SS316	SS316HT	18Ni300	18Ni300HT
Young modulus E [Gpa]	206	196	165	184
Proof strength 0.2% [Mpa]	600	540	1135	863
Rm [Mpa]	693	699	900	1293
Strain at break %	29.6	28.3	8	6

Figure 16: Tensile testing results.

Tensile tests

The effect of the heat treatment is also highlighted in the tensile test plots below. Indeed, the SS316 after heat treatment looks to yield at lower stresses then at the as-printed state. The opposite happens for the 18Ni300 because after quenching and aging treatments the tensile strength Rm significantly increases from 900 MPa to almost 1300 MPa. The mechanical properties of the tested samples are listed in Figure 16. Since the obtained results agree with the data in the literature, they can be considered reliable. As demonstrated, once a set of printing parameters that allows for high-quality component production is used, the mechanical properties of an additively manufactured part are not substantially different from those of conventionally manufactured parts.

Conclusions

Cold Spray

Erosion resistance to alumina particle impingement and electrochemical corrosion of a WC/Ni-Ni composite coating and a CrMnFeCoNi high entropy alloy coating were investigated compared to 440C steel performance. From the study, the following conclusions can be drawn:

- WC/Ni-Ni composite coating was successfully deposited on 2205 duplex stainless steel estimating a 43 vol% of entrapped WC particles.
- CrMnFeCoNi high entropy alloy was successfully deposited on a 316 stainless steel coating interlayer deposited on a 2205 duplex stainless steel substrate.
- After 1 hour of heat treatment at 600°C in air, the porosity of the WC/Ni-Ni coatings decreased from 1.4 vol% to 0.7 vol%, and the microhardness decreased from 370±58 to 252±39 HV0.5.

- After heat treatment, the porosity of the HEA coatings deposited on SS316, and heat-treated SS316 (HTSS316) was 1.8±0.4 vol% and 1.1±0.2 vol%, respectively. The average microhardness HV0.5 were 420±41 for the HEA on SS316 and 430±50 for the HEA on HTSS316.
- In general, as the impact angle was lowered, the mass loss of all samples increased, with the 30° condition proving to be the most critical of the experimental campaign.
- After heat treatment, the WC/Ni-Ni coating's erosion behaviour became less susceptible to variations in impact angle.
- At 60° impact angle, the as-sprayed WC/Ni-Ni coating exhibited the lowest erosion among the coating materials.
- The HEA on SS316 coating appears to have the highest strength against alumina particles impinging at 90° and 30° impact angles among the tested coating materials.
- However, the annealed 440C substrate shows a higher erosion resistance under alumina particles impingement but the corrosion tests highlighted a much stronger and quicker oxides penetration than in the coatings.

Selective Laser Melting

Optimal set of printing parameters were determined for Maraging steel 18Ni300 and Stainless steel 316 powders. Heat treatments effect on the behaviour under tensile tests was also investigated. From the study, the following conclusions can be drawn:

- Best set of parameters for Maraging steel printing was found to be at laser power of 240W, 1000 mm/s scanning speed and 70 µm hatch distance.
- Best set of parameters for 316 stainless steel printing was found to be at laser power of 210W, 1000 mm/s scanning speed and 70 µm hatch.
- After quenching and precipitation hardening heat treatments of the maraging 18Ni300 steel, the treatment significantly increased the sample hardness that improved from 399 HV0.5 to 566 HV0.5.
- After heat treatment at 600°C for 2 hours, the SS316 sample microhardness slightly decreased from 265 HV0.5 to 255 HV0.5.
- The heat treatments showed also to increase the tensile strength of the maraging steel and reducing the plasticity region of the stress-strain curve.
- For the 316 stainless steel, the heat treatment did not show a significant effect on the behaviour under tensile test.

References

[1] C. P. Paul, S. K. Mishra, P. Tiwari, and L. M. Kukreja, "Solid-Particle Erosion Behaviour of WC/Ni Composite Clad layers with Different Contents of WC Particles," *Opt. Laser Technol.*, vol. 50, pp. 155–162, 2013, doi: 10.1016/j.optlastec.2013.03.002.

[2] J. R. T. Branco, R. Gansert, S. Sampath, C. C. Berndt, and H. Herman, "Solid particle erosion of plasma sprayed ceramic coatings," *Mater. Res.*, vol. 7, no. 1, pp. 147–153, 2004, doi: 10.1590/s1516-14392004000100020.

[3] Y. Lian and Y. Li, "Investigation on erosion resistance of WC-Co-Cr coatings," *Tribol. Online*, vol. 13, no. 2, pp. 36–42, 2018, doi: 10.2474/trol.13.36.

[4] M. Kazasidis, E. Verna, S. Yin, and R. Lupoi, "The effect of heat treatment and impact angle on the erosion behavior of nickel-tungsten carbide cold spray coating using response surface methodology," *Emergent Mater.*, vol. 4, no. 6, pp. 1605–1618, 2021, doi: 10.1007/s42247-021-00274-7.

[5] V. K. Champagne, *The cold spray materials deposition process: Fundamentals and applications*. 2007.

[6] R. T. Sataloff, M. M. Johns, and K. M. Kost, *Modern Cold Spray*. Springer, 2015.

[7] G. Motors, S. N. Laborato-, and F. M. Company, *Cold spray technology*. .

[8] S. A. Alidokht and R. R. Chromik, "Sliding wear behavior of cold-sprayed Ni-WC composite coatings: Influence OF WC content," *Wear*, vol. 477, no. November 2020, p. 203792, 2021, doi: 10.1016/j.wear.2021.203792.

[9] S. Yin, E. J. Ekoi, T. L. Lupton, D. P. Dowling, and R. Lupoi, "Cold spraying of WC-Co-Ni coatings using porous WC-17Co powders: Formation mechanism, microstructure characterization and tribological performance," *Mater. Des.*, vol. 126, no. April, pp. 305–313, 2017, doi: 10.1016/j.matdes.2017.04.040.

[10] R. G. Rateick, K. R. Karasek, A. J. Cunningham, K. C. Goretta, and J. L. Routbort, "Solid-particle erosion of tungsten carbide/cobalt cermet and hardened 440C stainless steel-A comparison," *Wear*, vol. 261, no. 7–8, pp. 773–778, 2006, doi: 10.1016/j.wear.2006.01.012.

[11] C. J. Akisin, C. J. Bennett, F. Venturi, H. Assadi, and T. Hussain, "Numerical and Experimental Analysis of the Deformation Behavior of CoCrFeNiMn High Entropy Alloy Particles onto Various Substrates During Cold Spraying," *J. Therm. Spray Technol.*, vol. 31, no. 4, pp. 1085–1111, 2022, doi: 10.1007/s11666-022-01377-1.

[12] J. E. Ahn, Y. K. Kim, S. H. Yoon, and K. A. Lee, "Tuning the Microstructure and Mechanical Properties of Cold Sprayed Equiatomic CoCrFeMnNi High-Entropy Alloy Coating Layer," *Met. Mater. Int.*, vol. 27, no. 7, pp. 2406–2415, 2021, doi: 10.1007/s12540-020-00886-4.

[13] J. Mahaffey, A. Vackel, S. Whetten, M. Melia, and A. B. Kustas, "Structure Evolution and Corrosion Performance of CoCrFeMnNi High Entropy Alloy Coatings Produced Via Plasma Spray and Cold Spray," *J. Therm. Spray Technol.*, vol. 31, no. 4, pp. 1143–1154, 2022, doi: 10.1007/s11666-022-01373-5.

[14] R. Nikbakht *et al.*, "Cold Spray and Laser-Assisted Cold Spray of CrMnCoFeNi High Entropy Alloy Using Nitrogen as the Propelling Gas," *J. Therm. Spray Technol.*, vol. 31, no. 4, pp. 1129–1142, 2022, doi: 10.1007/s11666-022-01361-9.

[15] C. Wei, Z. Liu, Y. Bao, D. Wan, Y. Qiu, and X. Liu, "Evaluating thermal expansion coefficient and density of ceramic coatings by relative method," *Mater. Lett.*, vol. 161, pp. 542–544, 2015, doi: 10.1016/j.matlet.2015.09.034.

[16] Astm, "G76-07, Standard Test Method for Conducting

Erosion Tests by Solid Particle Impingement Using Gas Jets," *ASTM Int.*, vol. i, pp. 1–6, 2013, doi: 10.1520/G0076-18.2.

[17] Z. Mao, X. Lu, H. Yang, X. Niu, L. Zhang, and X. Xie, "Processing optimization, microstructure, mechanical properties and nanoprecipitation behavior of 18Ni300 maraging steel in selective laser melting," *Mater. Sci. Eng. A*, vol. 830, no. May 2021, p. 142334, 2022, doi: 10.1016/j.msea.2021.142334.

[18] M. Yakout, M. A. Elbestawi, and S. C. Veldhuis, "A study of thermal expansion coefficients and microstructure during selective laser melting of Invar 36 and stainless steel 316L," *Addit. Manuf.*, vol. 24, no. August, pp. 405–418, 2018, doi: 10.1016/j.addma.2018.09.035.

[19] S. A. Alidokht, P. Vo, S. Yue, and R. R. Chromik, "Cold Spray Deposition of Ni and WC-Reinforced Ni Matrix Composite Coatings," *J. Therm. Spray Technol.*, vol. 26, no. 8, pp. 1908–1921, 2017, doi: 10.1007/s11666-017-0636-4.

[20] M. Kazasidis, E. Verna, S. Yin, and R. Lupoi, "Investigation of the Effect of Low-Temperature Annealing and Impact Angle on the Erosion Performance of Nickel-Tungsten Carbide Cold Spray Coating Using Design of Experiments," *Therm. Spray 2022 Proc. from Int. Therm. Spray Conf.*, vol. 84369, pp. 763–772, 2022, doi: 10.31399/asm.cp.itsc2022p0763.

[21] S. Yin, J. Cizek, X. Yan, and R. Lupoi, "Annealing strategies for enhancing mechanical properties of additively manufactured 316L stainless steel deposited by cold spray," *Surf. Coatings Technol.*, vol. 370, no. April, pp. 353–361, 2019, doi: 10.1016/j.surfcoat.2019.04.012.

[22] S. Bagherifard *et al.*, "Tailoring cold spray additive manufacturing of steel 316 L for static and cyclic load-bearing applications," *Mater. Des.*, vol. 203, p. 109575, 2021, doi: 10.1016/j.matdes.2021.109575.

[23] K. H. Lo, F. T. Cheng, C. T. Kwok, and H. C. Man, "Effects of laser treatments on cavitation erosion and corrosion of AISI 440C martensitic stainless steel," *Mater. Lett.*, vol. 58, no. 1–2, pp. 88–93, 2004, doi: 10.1016/S0167-577X(03)00421-X.